CHALMERS
UNIVERSITY OF TECHNOLOGY

An adaptive finite element method for Fredholm integral equations of the first kind and its verification on experimental data

Cent. Eur. J. Math. • 11(8) • 2013 • 1489-1509
DOI: 10.2478/s11533-013-0247-3

VERSITA

Central European Journal of **Mathematics**

An adaptive finite element method for Fredholm integral equations of the first kind and its verification on experimental data

Research Article

Nikolay Koshev[1*], Larisa Beilina[2†]

1 Department of Physics, Penza State University of Architecture and Building, German Titov 28, 440028 Penza, Russian Federation

2 Department of Mathematical Sciences, Chalmers University of Technology and University of Gothenburg, Maskingränd 2, 42196 Gothenburg, Sweden

Received 30 July 2012; accepted 28 October 2012

Abstract: We propose an adaptive finite element method for the solution of a linear Fredholm integral equation of the first kind. We derive a posteriori error estimates in the functional to be minimized and in the regularized solution to this functional, and formulate corresponding adaptive algorithms. To do this we specify nonlinear results obtained earlier for the case of a linear bounded operator. Numerical experiments justify the efficiency of our a posteriori estimates applied both to the computationally simulated and experimental backscattered data measured in microtomography.

MSC: 65R20, 65R30, 65R32

Keywords: Fredholm integral equation of the first kind • Ill-posed problem • Adaptive finite element method • A posteriori error estimates • Tikhonov functional • Regularized solution

1. Introduction

In this work we consider solving a Fredholm integral equation of the first kind and propose an adaptive finite element method to solve it. Such problems arise in many applications of astrophysics [12], astronomy [5], image processing of smeared and defocused photography [23], image processing in microtomography [18] and spectroscopy in the backscattered

* *E-mail: nikolay.koshev@gmail.com*
† *E-mail: larisa@chalmers.se*

electron signal [10], etc. An adaptive finite element method for a Fredholm integral equation of the second kind was considered in [1]. In this paper we solve a more complicated and different problem: we derive a posteriori error estimates for a Fredholm integral equation of the first kind which is an ill-posed problem. Thus, to solve this problem, we need minimize the corresponding Tikhonov functional.

We will consider a Fredholm integral equation of the first kind which takes the form

$$\int_D K(t,s)z(s)\,ds = u(t), \qquad t \in D. \tag{1}$$

Here D is a closed bounded set in $\mathbb{R}^n$, $n = 2, 3$. It is assumed that the kernel $K(t,s)$ is the absolutely integrable function. Equation (1) can be written in an operator form as

$$A(z) = u \tag{2}$$

where $A\colon X \to Y$ and X and Y are complete metric spaces.

In the case when the kernel $K(t,s)$ in (1) is a smooth function then equations of type (1) are classified as ill-posed problems since the solution z is sensitive to the small perturbations in the data function u, see [12, 13, 19–21]. If the kernel $K(t,s)$ is a singular function then the ill-posedness in (1) is feasible. One of the examples of this type equation are the boundary integral equations used for solution of elliptic partial differential equations, see [2] and references therein. In this paper we consider the case when the operator A^{-1} in (2) is not a compact operator and thus we are dealing with a classic case of an ill-posed problem [20].

The main novelty of our work is in the derivation of a posteriori error estimates for the Tikhonov functional and for the regularized solution to this functional. These estimates are derived not only on the conforming finite element meshes where continuous piecewise linear functions CG(1) are applied but even on the meshes with hanging nodes. Thus we apply a discontinuous finite element method DG(1) on these meshes. To do that we specify results of [6–9, 16] for the case of the linear Fredholm integral equation of the first kind. Due to the linearity, the results of this paper are more clear than those of previous works and the proofs here are different from those of [6–9, 16]. Another novelty of this paper is that the Tikhonov regularization term is given in the H^1-norm, which is stronger than the L_2-norm being used in [6–9, 16]. These new moments cause additional difficulties compared with [6–9, 16].

We note that in [7, 8] *a posteriori* error estimates were obtained for the regularized coefficient rather than for the exact. In the follow-up work [16] the effect of the improvement in accuracy of the regularized coefficient was explained rather than the exact coefficient. More precisely, from [16] it follows that the regularized coefficient is closer to the exact coefficient than the first guess in the nonlinear case. Therefore, an improvement in the accuracy of the reconstruction of the regularized coefficient on the adaptively refined meshes leads to an improvement in the accuracy of the reconstruction of the exact solution. Similarly with [7, 8] we obtain new a posteriori error estimates for the regularized function.

The main concept of the adaptivity technique, which we apply to a Fredholm integral equation of the first kind, is explained below. In the case of ill-posed problems it is inefficient to use an exceedingly fine mesh in computations. The main idea of the adaptive finite element method is to obtain a good accuracy of solutions via local mesh refinements. In order to do this, we minimize the Tikhonov functional on a sequence of locally refined meshes. A posteriori error analysis developed in this paper addresses the main question in the adaptivity: where to refine the mesh locally in order to improve the resulting solution.

In our numerical examples we demonstrate the efficiency of the adaptivity technique for the image restoration problem of electron microscopy [18, 23]. The goal of our tests is to restore blurred images obtained in electron microscopy and identify possible defects on them. To do this we apply the adaptive algorithm of Section 8. Since in the computational examples of Section 9 we work only with a finite dimensional space of standard piecewise linear finite elements, we consider our problem in a finite dimensional space. However, the corresponding Fredholm integral equation of the first kind certainly inherits the ill-posed nature of its infinitely dimensional analog. Therefore, it is worth considering the Tikhonov functional.

In Tests 1 and 2 of Section 9 we have applied computationally simulated data, while in Test 3 real, measured data obtained by the microtomograph developed by Professor Eduard Rau at Moscow Lomonosov State University was

used [18, 23]. The conclusions from these tests is that the local adaptive mesh refinement algorithm can significantly improve the contrast of blurred images. In Test 2 of Section 9 we compare the performance of our adaptive algorithm with performance of methods of [17, 18] on the reconstruction of the deconvolution function. Our computational tests show that an adaptive finite element method gives better stability in the reconstruction of the deconvolution function.

Comparison with other techniques which are used for solution of such problems is presented in subsection 9.4. We compare three different reconstruction methods: the adaptive finite element method of this paper, the uniform grid deconvolution method of [23] and the Bounded Total Variation method of [18]. Test 4 demonstrates that an adaptive finite element method gives better results in the reconstruction of the high-intensive smeared images than the other two reconstruction methods. However the Bounded Total Variation method of [18] performs better in the case of large noise levels in the computational data on the reconstruction of non-intensive smeared images. Our conclusions is that the choice of the particular reconstruction method depends on the level of the noise in computational data and level of the smearing intensity of the image to be reconstructed.

We do not consider the case of multi-connected computational domains in this work. However, based on the results of Test 4 in subsection 9.4, it could be an interesting task to consider such domains in future research with different reconstruction methods applied in each domain.

The outline of this paper is as follows: In Section 2 we present the statement of the problem, the corresponding Tikhonov functional and its Frechét derivative. In Section 3 we describe CG(1) and DG(1) finite element spaces and present CG(1) and DG(1) finite element method for the Tikhonov functional. In Section 4 we demonstrate the general framework for a posteriori error estimates. A posteriori error estimates for the regularized solution on locally refined meshes are derived in Section 5 and a posteriori error estimates for the error in the Tikhonov functional are presented in Section 6. We formulate mesh refinement recommendations and adaptive algorithms in Sections 7, 8, respectively. Finally, in Section 9 we demonstrate the results of the reconstruction in two dimensions using adaptive algorithms of Section 8.

2. Notation used in the paper

We firstly introduce common notation which is used in this paper. Let $\Omega \subset \mathbb{R}^n$, $n = 2, 3$, be a bounded domain with the piecewise-smooth boundary $\partial\Omega$. In our numerical experiments we work with piecewise smooth boundaries and this is one of discrepancies between the theory and its numerical implementation.

Let function $u(x)$, $x = (x_1, \dots, x_n) \in \Omega$, be k times continuously differentiable in Ω. We denote the partial derivative of the order $|\alpha| \le k$ of u by

$$D^\alpha u = \frac{\partial^{|\alpha|} u}{\partial^{\alpha_1} x_1 \cdots \partial^{\alpha_n} x_n}, \qquad |\alpha| = \alpha_1 + \cdots + \alpha_n,$$

where $\alpha = (\alpha_1, \dots, \alpha_n)$ is such that $\alpha_i \ge 0$.

Let $C^k(\overline{\Omega})$ be the Banach space of functions $u(x)$ which are continuous in the closure $\overline{\Omega}$ of the domain Ω together with their derivatives $D^\alpha u$, $|\alpha| \le m$. The norm in this space is defined as

$$\|u\|_{C^k(\Omega)} = \sum_{|\alpha| \le m} \sup_{x \in \Omega} |D^\alpha u(x)| < \infty.$$

Let $H^k(\Omega)$ be a Hilbert space with the inner product defined as

$$(u, v)_{H^k(\Omega)} = \sum_{|\alpha| \le k} \int_\Omega D^\alpha u \, D^\alpha v \, dx$$

with the norm defined as

$$\|u\|^2_{H^k(\Omega)} = \sum_{|\alpha| \le k} \int_\Omega |D^\alpha u|^2 dx < \infty.$$

In $L_2(\Omega)$ the inner product and the norm are defined as

$$(u, v) = \int_\Omega uv \, dx, \qquad \|u\|^2 = (u, u).$$

2.1. Statement of the problem

Let H be the Hilbert space of functions defined in Ω. Recall that we consider $\Omega \subset \mathbb{R}^n$, $n = 2, 3$, which is a bounded domain with the piecewise-smooth boundary $\partial\Omega$. Our goal is to solve a Fredholm integral equation of the first kind

$$\int_\Omega \rho(x, y)z(x)\,dx = u(y), \qquad y \in \Omega, \tag{3}$$

where $u(y) \in L_2(\Omega)$, $z(x) \in H$, $\rho(x, y) \in C^k(\Omega \times \Omega)$, $k \geq 0$, is the kernel of the integral equation.

We can rewrite (3) in operator form as

$$A(z) = u \tag{4}$$

with an operator $A\colon H \to L_2(\Omega)$ defined as

$$A(z) = \int_\Omega \rho(x, y)z(x)\,dx. \tag{5}$$

Problem (P). Find the function $z(x) \in H$, $x \in \Omega$, satisfying (3) provided $\rho(x, y) \in C^k(\Omega \times \Omega)$, $k \geq 0$, and $u(y) \in L_2(\Omega)$ are known.

Although the function $A(z) \in C^k(\Omega)$, $k \geq 0$, we assume in (5) that $u \in L_2(\Omega)$. The reason for this is that the right hand side of this equation can exhibit noise.

2.2. The Tikhonov functional

We assume that the right hand side of (3) is given, with the small parameter $\delta \in (0, 1)$ which characterizes the level of the error in data. Let u^* be the perfect noiseless right hand side of (3) which corresponds to the exact solution z^* of (4) such that

$$A(z^*) = u^*, \qquad \|u - u^*\|_{L_2(\Omega)} \leq \delta.$$

Introduce the operator $F\colon H \to L_2$ such that

$$F(z) = Az - u.$$

Hence $Az^* - u^* = 0$. Since $\|u - u^*\|_{L_2(\Omega)} \leq \delta$ then

$$\|F(z^*)\|_{L_2(\Omega)} \leq \delta.$$

Recall that solving the operator equation (4) is a classical ill-posed problem [22] since the operator A^{-1} may not be compact. Thus, we assume that there exists the exact solution z^* to our problem (**P**), but we will never find this solution through computation. As a result we call the *regularized solution*, z_α, some approximation of the unknown exact solution z^* which satisfies the requirements of being close to the exact solution z^* and being stable with respect to the small errors of the right hand side $u(y)$ of equation (4). The algorithm for the solution to equation (4) can be written in the form $z_\alpha = R(\delta, \alpha)u$, where $R(\delta, \alpha)\colon L_2 \to H$ is the *regularization operator*, see in [22] for more information about construction of this operator. When we apply this operator to the solution of the ill-posed problem we get a *regularization algorithm*. In this paper we use the Tikhonov regularization algorithm which is based on the minimization of the Tikhonov functional. Thus to find regularized solution z_α to equation (3), we take $H = H^1$ and minimize the Tikhonov regularization functional $M_\alpha(z)$ in the form

$$M_\alpha(z) = \frac{1}{2}\|F(z)\|^2_{L_2(\Omega)} + \frac{\alpha}{2}\|z - z_0\|^2_{H^1(\Omega)}, \qquad M_\alpha\colon H^1 \to \mathbb{R}, \quad z_0 \in H^1, \tag{6}$$

where $\alpha = \alpha(\delta) > 0$ is a small regularization parameter. The choice of the point z_0 and the regularization parameter α depends on the concrete minimization problem which is outside of the scope of this publication. Usually z_0 is a good first approximation for the exact solution z^*.

From [22] it follows that an algorithm for the solution of equation (4), which is based on the minimization of the Tikhonov functional (6), is the regularization algorithm and the element $z_\alpha \in H^1$, where the functional (6) reaches its minimum, is the regularized solution.

Let us consider an important class of Fredholm integral equations of the first kind, the convolution equation. These equations can be presented in the form (4) with the convolution operator $A\colon H^1 \to L_2(\Omega)$ defined by

$$A(z) = \int_\Omega \rho(y-x)z(x)\,dx, \tag{7}$$

where $\rho(y-x) \in C^k(\Omega\times\Omega)$, $k \geq 0$, $z(x) \in H^1$. Using the convolution theorem and properties of the Fourier transform [21] we obtain the minimum $z(x) \in H^1$ of the functional (6) given by

$$z(x) = F^{-1}\left(\frac{\widehat{u}(\omega)\widehat{\rho}^*(\omega)}{|\widehat{\rho}(\omega)|^2 + \alpha(1+\omega^2)}\right), \tag{8}$$

where $\widehat{f}(\omega)$ denotes the Fourier transform $F(f)(\omega)$ of the function $f(\omega)$ defined by

$$\widehat{f}(\omega) = F(f)(\omega) = \frac{1}{(2\pi)^n}\int_{\mathbb{R}^n} f(x)e^{-i\omega x}\,dx.$$

We consider the convolution equation (7) in the numerical examples of Section 9. We note that our a posteriori error estimates are valid also for this type of equation.

2.3. The Fréchet derivative and the convexity of the Tikhonov functional

For convenience we introduce a more general form of the Tikhonov functional (6). This is done for the general form of the convexity property of this functional. Let W_1, W_2, Q be three Hilbert spaces, $Q \subseteq W_1$ as a set, the norm in Q is stronger than the norm in W_1 and $\overline{Q} = W_1$, where the closure is understood in the norm of W_1. We denote scalar products and norms in these spaces as $(\cdot,\cdot)$, $\|\cdot\|$ for W_1, $(\cdot,\cdot)_2$, $\|\cdot\|_2$ for W_2, and $[\cdot,\cdot]$, $[\cdot]$ for Q. Let $A\colon W_1 \to W_2$ be a bounded linear operator. Our goal is to find the function $z \in Q$ which minimizes the Tikhonov functional

$$J_\alpha(z)\colon Q \to \mathbb{R}, \qquad J_\alpha(z) = \frac{1}{2}\|Az-u\|_2^2 + \frac{\alpha}{2}[z-z_0]^2, \qquad u \in W_2, \quad z, z_0 \in Q, \tag{9}$$

where $\alpha \in (0,1)$ is the regularization parameter.

To do that we search for a stationary point of the above functional with respect to z satisfying for all $b \in Q$

$$J'_\alpha(z)(b) = 0, \tag{10}$$

where $J'_\alpha(z)$ is the Fréchet derivative of the functional (9) and $J'_\alpha(z)(b)$ means that J'_α acts on b.

The following lemma is well known [4] and we present it for the particular case when the operator $A\colon L_2 \to L_2$. In the case when $A\colon H^1 \to L_2$ the explicit derivation of the Fréchet derivative of the functional (9) is technically a more complicated problem because of the presence of the H^1-norm in the regularization term of the functional (9). We omit here the explicit presentation of the Fréchet derivative of the functional (9) in this case. However in the proofs of Theorems 5.1 and 6.1 the Fréchet derivative of the functional (9) is given in H^1 norm when the operator $A\colon H^1 \to L_2$.

Lemma 2.1.

Let $A\colon L_2 \to L_2$ be a bounded linear operator. Then the Fréchet derivative of the functional (9) is

$$J'_\alpha(z)(b) = (A^*Az - A^*u, b) + \alpha[z-z_0, b] \qquad \text{for all} \quad b \in Q.$$

In particular, for the integral operator (3) we have

$$J'_\alpha(z)(b) = \int_\Omega b(s)\left[\int_\Omega z(y)\left(\int_\Omega \rho(x,y)\rho(x,s)\,dx\right)dy - \int_\Omega \rho(x,s)u(x)\,dx\right]ds + \alpha[z-z_0,b] \qquad \text{for all} \quad b \in Q.$$

Lemma 2.2 is also well known since $A\colon W_1 \to W_2$ is a bounded linear operator. We again formulate this lemma only for our specific case, referring to [21] for a more general case. The situation is naturally more complicated for a nonlinear operator and we refer to [8] for this case.

Lemma 2.2.
Let the operator $A\colon W_1 \to W_2$ be a bounded linear operator which has the Fréchet derivative of the functional (9). Then the functional $J_\alpha(z)$ is strongly convex on the space Q and

$$\left(J'_\alpha(x) - J'_\alpha(z), x - z\right) \geq \alpha[x - z]^2 \qquad \text{for all} \quad x, z \in Q.$$

It is known from the theory of convex optimization that Lemma 2.2 implies existence and uniqueness of the global minimizer $z_\alpha \in Q$ of the functional J_α defined in (9) such that

$$J_\alpha(z_\alpha) = \inf_{z \in Q} J_\alpha(z).$$

It is well known that the operator F if is Lipschitz continuous

$$\|F(z_1) - F(z_2)\| \leq \|A\| \cdot \|z_1 - z_2\| \qquad \text{for all} \quad z_1, z_2 \in H.$$

We also introduce new constant $D = D(\|A\|, \alpha) = \text{const} > 0$ [3, 4] such that

$$\left\|J'_\alpha(z_1) - J'_\alpha(z_2)\right\| \leq D\|z_1 - z_2\| \qquad \text{for all} \quad z_1, z_2 \in H. \tag{11}$$

3. The finite element spaces and finite element method

Following [14] we discretize our bounded domain $\Omega \subset \mathbb{R}^n$, $n = 2, 3$, by an unstructured mesh T using non-overlapping elements K. In $\mathbb{R}^3$ the elements K are tetrahedrons and in $\mathbb{R}^2$ the elements K are triangles such that $T = K_1, \ldots, K_l$, where l is the total number of elements in Ω, and

$$\Omega = \bigcup_{K \in T} K = K_1 \cup K_2 \cup \cdots \cup K_l.$$

We associate the triangulation T with the mesh function $h = h(x)$, which is a piecewise-constant function such that

$$h(x) = h_K \qquad \text{for all} \quad K \in T,$$

where h_K is the diameter of K which we define as the longest side of K.

Let r' be the radius of the maximal circle/sphere contained in the element K. We make the following shape regularity assumption for every element $K \in T$:

$$a_1 \leq h_K \leq r' a_2, \qquad a_1, a_2 = \text{const} > 0.$$

We introduce now the finite element space V_h as

$$V_h = \left\{v(x) \in V : v \in C(\Omega),\ v\restriction_K \in P_1(K) \text{ for all } K \in T\right\},$$

where $P_1(K)$ denotes the set of piecewise-linear functions on K with $V = \{v(x) : v(x) \in H^1(\Omega)\}$. The finite dimensional finite element space V_h is constructed so that $V_h \subset V$. The finite element method uses piecewise-linear test functions which we call continuous Galerkin, or the CG(1) method. CG(1) can be applied on the conforming meshes.

In the general case we also allow meshes in a space with hanging nodes and assume that the local mesh size has bounded variation in such meshes. This means that there exists a constant $\gamma > 0$ such that $\gamma h_{K^+} \leq h_K \leq \gamma^{-1} h_{K^+}$ for all neighboring elements K^- and K^+. Let S be the internal face of the non-empty intersection of the boundaries of two neighboring elements K^+ and K^-. We denote the jump of the function v_h, computed from the two neighboring elements K^+ and K^-, sharing the common side S, as

$$[v_h] = v_h^+ - v_h^-.$$

We introduce the discontinuous finite element space W_h on such meshes as

$$W_h = \left\{v(x) \in V : v\restriction_K \in \mathrm{DP}_1(K) \text{ for all } K \in T\right\},$$

where $\mathrm{DP}_1(K)$ denotes the set of discontinuous linear functions on K. The finite element space W_h is constructed so that $W_h \subset V$. The finite element method which uses discontinuous piecewise-linear functions is called the DG(1) method.

Let M be a subspace of the space V. Let $P_h : V \to M$ for all $M \subset V$ be the operator of the orthogonal projection of V on M. Let the function $f \in H^1(\Omega) \cap C(\Omega)$ and $\partial_{x_i} f_{x_i} \in L_\infty(\Omega)$. We define f_k^I as the standard interpolant [11] on triangles/tetrahedra of the function $f \in H$. Then, by one of properties of the orthogonal projection,

$$\|f - P_h f\|_{L_2(\Omega)} \leq \|f - f_k^I\|_{L_2(\Omega)}.$$

It follows from [11, formula 76.3] that

$$\|f - P_h f\|_{L_2(\Omega)} \leq C_I \|h \nabla f\|_{L_2(\Omega)} \qquad \text{for all} \quad f \in V, \tag{12}$$

where $C_I = C_I(\Omega)$ is a positive constant depending only on the domain Ω.

The CG(1) finite element method reads: find $z_h \in V_h$ satisfying (10) for all $b \in V_h$. The DG(1) finite element method reads: find $z_h \in W_h$ satisfying (10) for all $b \in W_h$.

4. General framework of a posteriori error estimates

Our goal is to present a posteriori error estimates for two kinds of error:

- For the error $|J_\alpha(z_\alpha) - J_\alpha(z_h)|$ in the Tikhonov functional (9).
- For the error $|z_\alpha - z_h|$ in the regularized solution to this functional, z_α.

To achieve the first goal, we note that

$$J_\alpha(z_\alpha) - J_\alpha(z_h) = J'_\alpha(z_h)(z_\alpha - z_h) + R(z_\alpha, z_h),$$

where $R(z_\alpha, z_h)$ is the second order remainder term. We assume that z_h is located in the small neighborhood of the regularized solution z_α. Thus, the term $R(z_\alpha, z_h)$ is small and can be neglected.

We now use the Galerkin orthogonality principle

$$J'_\alpha(z_h)(b) = 0 \qquad \text{for all} \quad b \in V_h \quad \text{or for all} \quad b \in W_h$$

together with the splitting

$$z_\alpha - z_h = (z_\alpha - z_\alpha^I) + (z_\alpha^I - z_h),$$

where $z_\alpha^I \in V_h$ or $z_\alpha^I \in W_h$ is the interpolant of z_α, and get the following error representation:

$$J_\alpha(z_\alpha) - J_\alpha(z_h) \approx J'_\alpha(z_h)(z_\alpha - z_\alpha^I). \tag{13}$$

A posteriori error estimate (13) involves the derivative of the Tikhonov functional $J'_\alpha(z_h)$ which represents the residual multiplied by weights $z_\alpha - z_\alpha^I$.

To derive the error $z_\alpha - z_h$, in the regularized solution z_α we use the convexity property of the Tikhonov functional (9) together with the interpolation property (12). We now make both error estimates more explicit for the case of CG(1) and DG(1) applied to the solution of (3).

5. An a posteriori error estimate of the regularized solution for refined meshes

In this section we formulate a theorem for an a posteriori error estimate for the regularized solution z_α for the case of the functional M_α defined in (6). This theorem is also valid in the common case where the functional $J_\alpha(z)$ is defined as in (9). Not to abuse notation in the proof of this theorem we denote the scalar product $(\cdot,\cdot)_{H^1}$ by $(\cdot,\cdot)$.

Theorem 5.1.
Let $z_h \in W_h$ be a finite element approximation of the regularized solution $z_\alpha \in H^2(\Omega)$ on the finite element mesh T with the mesh function h. There then exists a constant D defined by (11) such that the following a posteriori error estimate for the regularized solution z_α holds:

$$\|z_h - z_\alpha\|_{H^1(\Omega)} \le \frac{D}{\alpha} C_I \Big(\|h z_h\|_{L_2(\Omega)} + \|[z_h]\|_{L_2(\Omega)} + C \max_{S\subset\partial K} h_K^{-1} \|[\partial_S z_h]\|_{L_2(\Omega)} \Big) \qquad \text{for all} \quad z_h \in W_h. \tag{14}$$

In the case when $z_h \in V_h$ we have an a posteriori error estimate

$$\|z_h - z_\alpha\|_{H^1(\Omega)} \le \frac{D}{\alpha} C_I \|h z_h\|_{L_2(\Omega)}. \tag{15}$$

Proof. Let z_h be the minimizer of the Tikhonov functional (6). The existence and uniqueness of this minimizer are guaranteed by Lemma 2.2. Since by Lemma 2.2 the functional (6) is strongly convex on the space H^1 with the strong convexity constant α, this fact implies that

$$\alpha \|z_h - z_\alpha\|^2_{H^1(\Omega)} \le \big(M'_\alpha(z_h) - M'_\alpha(z_\alpha), z_h - z_\alpha \big), \tag{16}$$

where $M'_\alpha(z_h), M'_\alpha(z_\alpha)$ are the Fréchet derivatives of the functional (6) for the operator $A\colon H^1 \to L_2$.

Since z_α is the minimizer on the set H^1, then

$$(M'_\alpha(z_\alpha), z) = 0 \qquad \text{for all} \quad z \in H^1.$$

Using (16) with the splitting

$$z_h - z_\alpha = (z_h - P_h z_\alpha) + (P_h z_\alpha - z_\alpha),$$

together with the Galerkin orthogonality principle

$$\big(M'_\alpha(z_h) - M'_\alpha(z_\alpha), z_h - P_h z_\alpha \big) = 0$$

such that either $(z_h, P_h z_\alpha) \in V_h$ for CG(1) or $(z_h, P_h z_\alpha) \in W_h$ for DG(1), we obtain

$$\alpha \|z_h - z_\alpha\|^2_{H^1} \leq \left(M'_\alpha(z_h) - M'_\alpha(z_\alpha), P_h z_\alpha - z_\alpha\right). \tag{17}$$

We can estimate the right hand side of (17) using (11) as

$$\left(M'_\alpha(z_h) - M'_\alpha(z_\alpha), P_h z_\alpha - z_\alpha\right) \leq D \|z_h - z_\alpha\|_{H^1(\Omega)} \|P_h z_\alpha - z_\alpha\|_{H^1(\Omega)}.$$

Substituting the above equation into (17) we obtain

$$\|z_h - z_\alpha\|_{H^1(\Omega)} \leq \frac{D}{\alpha} \|P_h z_\alpha - z_\alpha\|_{H^1(\Omega)}.$$

Using the interpolation property

$$\|P_h z_\alpha - z_\alpha\|_{H^1(\Omega)} \leq C_I \|h z_\alpha\|_{H^2(\Omega)}$$

we obtain an a posteriori error estimate for the regularized solution with the interpolation constant C_I,

$$\|z_h - z_\alpha\|_{H^1(\Omega)} \leq \frac{D}{\alpha} \|P_h z_\alpha - z_\alpha\|_{H^1(\Omega)} \leq \frac{D}{\alpha} C_I \|h z_\alpha\|_{H^2(\Omega)}.$$

We can estimate $\|h z_\alpha\|_{H^2(\Omega)}$ as

$$\begin{aligned} \|h z_\alpha\|_{H^2(\Omega)} &\leq \sum_K \|h_K z_\alpha\|_{H^2(K)} = \sum_K \left\|(z_\alpha + \nabla z_\alpha + D^2 z_\alpha) h_K\right\|_{L_2(K)} \\ &\leq \sum_K \left(\|z_h h_K\|_{L_2(K)} + \left\| \frac{[z_h]}{h_K} h_K \right\|_{L_2(K)} + \left\| \frac{[\partial_{n_K} z_h]}{h_K} h_K \right\|_{L_2(\partial K)} \right) \\ &\leq \|h z_h\|_{L_2(\Omega)} + \sum_K \left(\|[z_h]\|_{L_2(K)} + \|[\partial_{n_K} z_h]\|_{L_2(\partial K)} \right). \end{aligned} \tag{18}$$

The second order derivatives of z_α are denoted in (18) by $D^2 z_\alpha$, ∂K denotes the boundary of element K, $[\partial_{n_K} z_h]$ is the jump of the normal derivative of the function z_h in the outward direction n_K, $[z_h]$ is the jump of the function z_h over the element K and h_K is the diameter of the element K. In (18) we also used the fact that [15]

$$|\nabla z_\alpha| \leq \frac{\|[z_h]\|}{h_K} \qquad \text{and} \qquad |D^2 z_\alpha| \leq \frac{\|[\partial_{n_K} z_h]\|}{h_K}.$$

We now estimate the third and second terms in the last row of (18). We sum over the element boundaries such that every internal side S of the element K occurs twice. We denote $\partial_S z_h$ as the derivative of the function z_h in one of the normal directions of every side S to get

$$\sum_K \|[\partial_{n_K} z_h]\|_{L_2(\partial K)} = \sum_S \|[\partial_S z_h]\|_{L_2(S)}, \tag{19}$$

where $[\partial_S z_h]$ is the jump in the derivative $\partial_S z_h$ computed from the two triangles sharing the same side S. We now distribute every jump equally over the two triangles sharing the side S and return to the sum over the elements boundaries ∂K to get

$$\sum_S \|[\partial_S z_h]\|_{L_2(S)} = \sum_K \frac{1}{2} h_K^{-1} \|[\partial_S z_h] h_K\|_{L_2(\partial K)}. \tag{20}$$

Now we replace the norms over the element boundaries ∂K by the norm over the domain Ω to get

$$\left| \sum_K \frac{1}{2} h_K^{-1} \|[\partial_S z_h] h_K\|_{L_2(\partial K)} \right| \leq C \max_{S \subset \partial K} h_K^{-1} \|[\partial_S z_h]\|_{L_2(\Omega)} \tag{21}$$

with the constant $C > 0$.

Substituting the above estimates into the right hand side of (18) we get (14). In the case when the $z_h \in V_h$ terms with jumps disappear, we have the a posteriori error estimate (15). □

6. A posteriori error estimates for the functional (6)

In Theorem 6.1 we derive a posteriori error estimates for the error in the Tikhonov functional (6) on the finite element mesh T. This theorem is also valid for the common case of the functional $J_\alpha(z)$ in (9).

Theorem 6.1.
Suppose that there exists a minimizer $z_\alpha \in H^2(\Omega)$ of the functional M_α on the set V and mesh T. Suppose also that there exists finite element approximation z_h of the minimizer z_α of M_α on the set W_h and mesh T with the mesh function h. Then for all $z_h \in W_h$ the following approximate a posteriori error estimate for the error $e = |M_\alpha(z_\alpha) - M_\alpha(z_h)|$ in the Tikhonov functional (6) holds:

$$e = |M_\alpha(z_\alpha) - M_\alpha(z_h)| \le C_l \|M'_\alpha(z_h)\|_{H^1(\Omega)} \left(\|hz_h\|_{L_2(\Omega)} + \|[z_h]\|_{L_2(\Omega)} + C \max_{S \subset \partial K} h_K^{-1} \|[\partial_S z_h]\|_{L_2(\Omega)} \right). \tag{22}$$

In the case when the finite element approximation $z_h \in V_h$ we have following a posteriori error estimate:

$$e = |M_\alpha(z_\alpha) - M_\alpha(z_h)| \le C_l \|M'_\alpha(z_h)\|_{H^1(\Omega)} \|hz_h\|_{L_2(\Omega)}. \tag{23}$$

Proof. By definition of the Frechét derivative we can write that on the mesh T,

$$M_\alpha(z_\alpha) - M_\alpha(z_h) = M'_\alpha(z_h)(z_\alpha - z_h) + R(z_\alpha, z_h), \tag{24}$$

where by Lemma 2.1, $R(z_\alpha, z_h) = O((z_\alpha - z_h)^2)$, as $z_\alpha - z_h \to 0$, for all $z_\alpha, z_h \in V$ and $M'_\alpha(z_h)$ is the Fréchet derivative of the functional (6) for the operator $A\colon H^1 \to L_2$. The term $R(z_\alpha, z_h)$ is small since we assume that z_h is the minimizer of the Tikhonov functional on the mesh T, this minimizer is located in a small neighborhood of the regularized solution z_α. Thus, we can neglect R in (24), see similar results for the case of a general nonlinear operator equation in [4, 8]. Next, we use the splitting

$$z_\alpha - z_h = z_\alpha - z_\alpha^l + z_\alpha^l - z_h$$

and the Galerkin orthogonality [11]

$$M'_\alpha(z_h)(z_\alpha^l - z_h) = 0 \qquad \text{for all} \quad z_\alpha^l, z_h \in W_h,$$

to get

$$M_\alpha(z_\alpha) - M_\alpha(z_h) \le M'_\alpha(z_h)(z_\alpha - z_\alpha^l),$$

where z_α^l is the standard interpolant of z_α on the mesh T [11]. We have that

$$|M_\alpha(z_\alpha) - M_\alpha(z_h)| \le \|M'_\alpha(z_h)\|_{H^1(\Omega)} \|z_\alpha - z_\alpha^l\|_{H^1(\Omega)}, \tag{25}$$

where the term $\|z_\alpha - z_\alpha^l\|_{H^1(\Omega)}$, in the right hand side of the above inequality, can be estimated using the interpolation estimate with the constant C_l

$$\|z_\alpha - z_\alpha^l\|_{H^1(\Omega)} \le C_l \|hz_\alpha\|_{H^2(\Omega)}.$$

Substituting the above estimate into (25) we get

$$|M_\alpha(z_\alpha) - M_\alpha(z_h)| \le C_l \|M'_\alpha(z_h)\|_{H^1(\Omega)} \|hz_\alpha\|_{H^2(\Omega)}.$$

Using the fact that [15]

$$|\nabla z_\alpha| \le \frac{|[z_h]|}{h_K} \qquad \text{and} \qquad |D^2 z_\alpha| \le \frac{|[\partial_n z_h]|}{h_K},$$

we can estimate $\|hz_\alpha\|_{H^2(\Omega)}$ using a similar technique to (18)–(21), to get (22). In the case when $z_h \in V_h$ all terms with jumps in (22) disappear and we get estimate (23). □

7. Mesh refinement recommendations

Using Theorems 5.1 and 6.1 we now formulate our mesh refinement recommendations which are used in Section 9 to improve the accuracy of the reconstruction of the regularized solution z_α of (**P**).

Estimate (14) of Theorem 5.1 provides an idea of where we need to refine the mesh locally in order to improve the accuracy of the regularized solution z_α. Given a finite element approximation $z_h \in W_h$ of the regularized solution $z_\alpha \in H^2(\Omega)$, the main impact of the norms in the computed finite element solution z_h in estimate (14) are provided by neighborhoods of the points in the finite element mesh T where $\|hz_h\|_{L_2(\Omega)}$ achieves its maximal value. We note that additional terms with jumps in estimate (14) disappear in the case of the conforming finite element meshes when $z_h \in V_h$. Thus the first idea for the finite element mesh refinement is the neighborhoods of all points in the finite element mesh T where the function $|hz_h|$ achieves its maximum should be refined.

Similarly, estimate (22) of Theorem 6.1 provides the second idea of where to refine the finite element mesh locally in order to improve the accuracy in the Tikhonov functional (6). Given a finite element approximation $z_h \in W_h$ of the regularized solution $z_\alpha \in H^2(\Omega)$ and the computed Frechét derivative $M'_\alpha(z_h)$ of the Tikhonov functional (6), the main impact of the norms given in the right hand side of the estimate (22), are provided by neighborhoods of the points in the finite element mesh T where both norms $\|hz_h\|_{L_2(\Omega)}$ and $\|M'_\alpha(z_h)\|_{H^1(\Omega)}$ achieve their maximal value. Thus the second idea for the finite element mesh refinement is the neighborhoods of all points in the finite element mesh T where $|M'_\alpha(z_h)|$ achieves its maximum or both functions $|hz_h|$ and $|M'_\alpha(z_h)|$ achieve their maximum should be refined.

Since the term $|hz_h|$ is already included in the first mesh refinement recommendation, we write only one term $|M'_\alpha(z_h)|$ in the second mesh refinement recommendation. Thus, by combining the first and second mesh refinement recommendations we can perform numerical tests to check performance of different mesh refinement criteria.

Since Theorems 5.1 and 6.1 are valid for the common case of the functional $J_\alpha(z)$ defined in (9), we write the second mesh refinement recommendation for this functional.

The First Mesh Refinement Recommendation.

Using Theorem 5.1 we conclude that we should refine the mesh in neighborhoods of those points in Ω where the function $|hz_h|$ attains its maximal values, more precisely in such subdomains of Ω where

$$|hz_h| \geq \widetilde{\varkappa} \max_{\Omega} |hz_h|,$$

where $\widetilde{\varkappa} \in (0,1)$ is the number which should be chosen computationally and h is the mesh function of the finite element mesh T.

The Second Mesh Refinement Recommendation.

Using Theorem 6.1 we conclude that we should refine the mesh in neighborhoods of those points in Ω where the function $|J'_\alpha(z_h)|$ attains its maximal values. More precisely, let $\varkappa \in (0,1)$ be the tolerance number which should be chosen in computational experiments. Refine the mesh in such subdomains of Ω where

$$|J'_\alpha(z_h)| \geq \varkappa \max_{\Omega} |J'_\alpha(z_h)|.$$

8. The adaptive algorithm

In this section we present two adaptive algorithms for the solution of a Fredholm integral equation of the first kind (3) which we apply in the numerical examples of Section 9. In our algorithms we define the minimizer and its computed solution, or approximation, on the k times refined mesh T_k by z_α and z_k, respectively. In our mesh refinement recommendations we need to compute the function z_k. To do that we use the convolution theorem (34) of Section 9. In Algorithm 1 we apply the modified second mesh refinement recommendation of Section 7, whilst in Algorithm 2 we use both mesh refinement recommendations of Section 7. These algorithms have been successfully tested, shown by the numerical examples of Section 9.

Algorithm 1.

Choose an initial mesh T_0 in Ω and obtain the numerical solution z_0 of (6) for T_0 using the finite element discretization of (10), with $b \in V_h$, for CG(1) or (10), with $b \in W_h$, for DG(1), and discretization of convolution theorem (34). Compute the sequence $z_k, k > 0$, on a refined mesh T_k using the following steps:

Step 1. Obtain the numerical solution z_k of (6) for T_k using the finite element discretization of (10), with $b \in V_h$, for CG(1) or (10), with $b \in W_h$, for DG(1) and the discretization theorem (34).

Step 2. Refine the mesh T_k at all points where

$$|B_h(z_k)| \geq \beta_k \max_{\Omega} |B_h(z_k)|,$$

where we define the a posteriori error indicator $B_h(z_k)$ as

$$B_h(z_k) = \int_{\Omega} z_k(y) \left(\int_{\Omega} \rho(x,y)\rho(x,s)\,dx \right) dy - \int_{\Omega} \rho(x,s)\,u(x)\,dx. \tag{26}$$

Here the tolerance number $\beta_k \in (0,1)$ is chosen by the user. Construct a new mesh T_{k+1} in Ω.

Step 3. Perform Steps 1–2 on the new mesh. Stop mesh refinements when $\|z_k - z_{k-1}\| < \epsilon$ or $\|B_h(z_k)\| < \epsilon$, where ϵ is tolerance chosen by the user. To compute norms $\|z_k - z_{k-1}\|$, the solution z_{k-1} is interpolated from the mesh T_{k-1} to the mesh T_k.

Algorithm 2.

Choose an initial mesh T_0 in Ω and obtain the numerical solution z_0 of (6) for T_0 using the finite element discretization of (10), with $b \in V_h$, for CG(1) or (10), with $b \in W_h$, for DG(1), and the convolution theorem (34). Compute the sequence z_k, $k > 0$, using the following steps:

Step 1. Obtain the numerical solution z_k of (6) on T_k using the finite element discretization of (10), with $b \in V_h$, for CG(1) or (10), with $b \in W_h$, for DG(1) and the discretization theorem (34).

Step 2. Refine the mesh T_k at all points where

$$|B_h(z_k)| \geq \beta_k \max_{\Omega} |B_h(z_k)|$$

with the a posteriori error indicator $B_h(z_k)$ defined by (26), and where

$$|z_k(x)| \geq \widetilde{\varkappa}_k \max_{\Omega} |z_k(x)|. \tag{27}$$

Here the tolerance numbers $\beta_k, \widetilde{\varkappa}_k \in (0,1)$ are chosen by the user. Construct a new mesh T_{k+1} in Ω.

Step 3. Perform Steps 1–2 on the new mesh. Stop mesh refinements when $\|z_k - z_{k-1}\| < \epsilon$ or $\|B_h(z_k)\| < \epsilon$, where ϵ is tolerance chosen by the user. To compute the norms $\|z_k - z_{k-1}\|$, the solution z_{k-1} is interpolated from the mesh T_{k-1} to the mesh T_k.

Remarks.

1. We note that the choice of the tolerance numbers $\beta_k, \widetilde{\varkappa}_k$ in (26), (27) depends on the concrete values of $\max_{\Omega} |B_h(z_k)|$ and $\max_{\Omega} |z_k(x)|$, respectively. If we choose $\beta_k, \widetilde{\varkappa}_k$ to be very close to 1 then we would refine the mesh in a very narrow region of the computational domain Ω and if we choose $\beta_k, \widetilde{\varkappa}_k \approx 0$ then almost all of the mesh in the domain Ω will be refined, which is unsatisfactory. Thus, the values of the numbers $\beta_k, \widetilde{\varkappa}_k$ should be chosen in an optimal way. Our numerical tests of Section 9 show that the choice of $\beta_k, \widetilde{\varkappa}_k = 0.5$ is almost optimal, since with this choice of the parameters $\beta_k, \widetilde{\varkappa}_k$, the finite element mesh is refined exactly at the places where we computed the function z_h, see Figures 1, 2, 4. However, such choice of numbers $\beta_k, \widetilde{\varkappa}_k$ is valid for our computational tests of Section 9 and it can be changed during the iterations in adaptive algorithms from a coarser to a more refined mesh.

2. We also note that we neglect the computation of the regularization term in the a posteriori error indicator (26) since this term is very small and does not affect the refinement procedure. However, this term is included in the minimization procedure of the Tikhonov functional (6).

9. Numerical studies of the adaptivity technique in microtomography

In all our tests of this section we consider the problem of the two-dimensional reconstruction of the backscattered signal in microtomography [18, 23]. This method allows non-destructive layer-by-layer image restoration of micro and nanostructures, for example, reconstruction of integral microschemes.

In the numerical tests of this section we show examples of the image restoration in microtomography using the adaptive finite element method with piecewise linear functions on locally refined meshes. We present numerical studies of the adaptive algorithms of Section 8 on the computationally simulated data (Tests 1, 2 in subsection 9.2) and on the experimental data (Test 3 in subsection 9.3). In Test 2 of subsection 9.2 we also compare results obtained by the uniform deconvolution algorithm of [18, 23] with the adaptivity technique of this paper.

The experimental backscattered signal in Test 3 of subsection 9.3 is generated by the microtomograph developed by Eduard Rau. This device is based on the electron microscope working in the backscattering electron mode. As soon as the original measured images are obtained by the microtomograph they can be improved by mathematical methods. It is well known that in mathematics the problem of image restoration in microtomography consists of solving a Fredholm integral equation of the first kind which is ill-posed problem. The usual method for solving this equation in two and three dimensions is minimizing the Tikhonov functional (6) in some bounded domain $\Omega \subset \mathbb{R}^n$, $n = 2, 3$, using the deconvolution algorithm on the uniform mesh [18, 23].

In Test 4 of subsection 9.4 we compare three different reconstruction methods: the adaptive finite element method of this paper, the uniform grid deconvolution method of [23] and the Bounded Total Variation method of [18]. Our tests show that the relative computational error in the adaptive finite element method is smaller than the other two methods for the reconstruction of high-intensive smeared images. However, the Bounded Total Variation method of [18] gives the smallest relative error in the case of increasing noise levels in the computational data for the reconstruction of non-intensive smeared images.

We can conclude that the choice of the numerical reconstruction method depends on the concrete real application, the level of the noise in the computational data and the smearing intensity of the image to be reconstructed.

9.1. Statement of the problem

Reconstruction in microtomography is based on analyzing the energy loss of the electrons backscattered by a layer of some solid object under investigation. Usually the electron probe (monokinetic electron ray) falls normally to the surface of the object. Since electrons are reflected from different depths of the object, they have different energies such that we can filter them using these energies. Thus, we can get the backscattered signal only from the depth in which we are interested.

The measured intensity of the signal depends on the scattering coefficient of the material of the object. This intensity is saved into the point of a plane image which corresponds to the position of the electron probe. Collecting all intensities at all points over the domain where we measure our signal into some matrix, we can obtain the image of the distribution of the intensity in the domain under investigation.

Unfortunately, the image formed in this way has drawbacks. One of them is blurring which can be explained by the fact that the finite radius of the electron probe leads to the situation when every position of the electron probe produces some spot in the matrix, where the signal is saved.

Let us denote r_0 as the known radius of the primary electron beam outside the target. The radius r of the electron probe for the penetration depth d can be represented using the empirical formula

$$(r'(d))^2 = r_0^2 + 0.625 \frac{Z}{E_0} \left(\frac{k}{A} \right)^{0.5} d^{1.5}, \tag{28}$$

where Z and A are the atomic number and the atomic weight respectively. Here, r' and d are expressed in centimeters [cm], energy E_0 in kelvin [keV] and the density of the material of the target k in gram/centimeter^3 [g/cm^3].

The distribution of the current density in the cross section of the electron probe can be represented by a Gauss distribution [18]. This distribution transforms the depth d with the scaling parameter (dispersion) $r'(d)$ defined by (28). For short notation we define $r(d)$ as the radius of the electron probe. Thus, the distribution of the current density $\rho(r)$ can be calculated using the expression

$$\rho(r) = \frac{1}{2\pi r'^2} \exp\left(-\frac{r^2}{2r'^2}\right). \tag{29}$$

The distribution of the current density $\rho(x_1, x_2)$ in the Cartesian coordinate system (x_1Ox_2) which is defined in the plane of the layer under investigation, can be defined by the formula

$$\rho(x_1, x_2) = \frac{1}{2\pi r'^2} \exp\left(-\frac{x_1^2 + x_2^2}{2r'^2}\right). \tag{30}$$

The signal distribution via the frame is formed line by line through the integral measuring of the intensity of the backscattered electron signal. The measured intensity is saved into the point of a plane image, which corresponds to the position of the electron probe.

Let $z(x_1, x_2)$ be the scattering coefficient at the point with coordinates (x_1, x_2). Let $(\xi O\eta)$ be another Cartesian coordinate system which is defined in the plane of the image. Without loss of generality we can assume that this system is equivalent to the system (x_1Ox_2). If the electron probe is located at some point (ξ, η) in the layer under investigation, then the intensity at this point is proportional to the number of electrons backscattered from the object.

Let Ω be the bounded domain representing the object under investigation. We decompose this domain into N small rectangular subdomains ω_i such that $\Omega = \bigcup_{i=1}^{N} \omega_i$, $\omega_i \cap \omega_j = \emptyset$ for all $i \neq j$. Let subdomains ω_i have sizes dx_1, dx_2 such that $\omega_i = dx_1 \times dx_2$ and the point $(x_1, x_2) \in \omega_i$. We assume a constant scattering coefficient $z(x_1, x_2)$ inside every subdomain ω_i when $dx_1 \to 0$ and $dx_2 \to 0$. Thus the backscattered signal over the domain ω_i at the point (ξ, η) is proportional to the current density $\rho(x_1 - \xi, x_2 - \eta)$ of the electron probe and to the scattering coefficient $z(x_1, x_2)$ at the point (x_1, x_2). This signal can be described by the equation

$$u(\xi, \eta) = z(x_1, x_2)\rho(x_1 - \xi, x_2 - \eta)\, dx_1\, dx_2. \tag{31}$$

Integrating (31) over all subdomains $\omega_i \subset \Omega$ and summing them over the computational domain Ω we get expression for the backscattered signal $u(\xi, \eta)$ at the point (ξ, η) in the whole domain Ω,

$$u(\xi, \eta) = \int_{\Omega} z(x_1, x_2)\rho(x_1 - \xi, x_2 - \eta)\, dx_1\, dx_2. \tag{32}$$

Inverse Problem (IP). Find the function $z(x_1, x_2) \in H^1$, $(x_1, x_2) \in \Omega$, satisfying (32) provided functions $\rho(x_1 - \xi, x_2 - \eta) \in C^k(\Omega \times \Omega)$, $k \geq 0$, and $u(\xi, \eta) \in L_2(\Omega)$ are known.

We note that equation (32) is a Fredholm integral equation of the first kind in two dimensions. It can be presented in the form (4) with the convolution operator $A\colon H^1 \to L_2(\Omega)$ defined by

$$A(z) = \int_{\Omega} \rho(x_1 - \xi, x_2 - \eta) z(x_1, x_2)\, dx_1\, dx_2.$$

To solve the inverse problem (**IP**) we minimize the Tikhonov functional (6) in the form

$$M_\alpha(z) = \left\| \int_{\Omega} \rho(x_1 - \xi, x_2 - \eta) z(x_1, x_2)\, dx_1\, dx_2 - u(\xi, \eta) \right\|^2_{L_2(\Omega)} + \alpha \|z(x_1, x_2)\|^2_{H^1}. \tag{33}$$

Using the convolution theorem and the properties of a Fourier transform [20, 21] in a similar way to (8), we can obtain the following formula for the minimizer $z_\alpha(x_1, x_2)$ of the functional (33) in two dimensions:

$$z_\alpha(x_1, x_2) = \int_{\mathbb{R}^2} e^{-i(\lambda x_1 + \nu x_2)} \frac{\widehat{\rho}^*(\lambda, \nu)\widehat{u}(\lambda, \nu)}{|\widehat{\rho}(\lambda, \nu)|^2 + \alpha(1 + \lambda^2 + \nu^2)}\, d\lambda\, d\nu, \tag{34}$$

where functions $\widehat{u}$ and $\widehat{\rho}$ are the Fourier transforms of the functions u and ρ, respectively.

In [17, 18] the solution to equation (32) was found on uniform grids on spaces H^1 and VH(B) (the space of functions with bounded total variation). The best reconstruction result was obtained using the bounded total variation functions, taking the first approximation in the H^1 space. Our computational tests of subsection 9.2 show better stability of the adaptive method than the methods of [17, 18].

9.2. Tests with simulated backscattered data

The goal in Test 1 and 2 was to solve (**IP**) and restore the function $z(x_1, x_2)$ in (32) under the condition that we know functions $\rho(x_1 - \xi, x_2 - \eta) \in C^k(\Omega \times \Omega)$, $k \geq 0$, and $u(\xi, \eta) \in L_2(\Omega)$ in (32). The function $\rho(x_1 - \xi, x_2 - \eta)$ is given by (30), and the function $u(\xi, \eta)$ represents the backscattered signal. In all our tests we decompose the finite element domain Ω into non-overlapping triangles as described in Section 3.

In Tests 1–3 we used simulated backscattered data $u(\xi, \eta)$. More precisely, we compute the function $u(\xi, \eta)$ in (32) using the known functions $z(x_1, x_2)$ and $\rho(x_1 - \xi, x_2 - \eta)$ in (32). Next, the function $z(x_1, x_2)$ is "forgotten" and our goal is to reconstruct this function for all $(x_1, x_2) \in \Omega$ by known functions $\rho(x_1 - \xi, x_2 - \eta)$ and $u(\xi, \eta) \in L_2(\Omega)$ in (32).

We define an a posteriori error indicator (26) for (**IP**) as

$$B_h(z_k) = \int_\Omega z_k(\xi, \eta) \left(\int_\Omega \rho(x_1 - \xi, x_2 - \eta) \rho(x_1 - s_1, x_2 - s_2)\, dx_1\, dx_2 \right) d\xi\, d\eta - \int_\Omega \rho(x_1 - s_1, x_2 - s_2) u(x_1, x_2)\, dx_1\, dx_2, \quad (35)$$

where Ω is our two-dimensional computational domain. Recall that according to Remark 2 we omit the computation of the regularization term in the indicator (35) since this term is negligible compared to other terms presented. Thus, this term does not affect refinement of the mesh.

Test 1-a). The computational domain Ω in this test has area $S_\Omega = 3.4813$ mkm (1 micrometre mkm $= 1 \cdot 10^{-6}$ of a metre). The backscattered signal is the simulated function $u(\xi, \eta)$ in (32) which is presented in Figure 1-a). This is computed for the function $\rho(x_1 - \xi, x_2 - \eta)$ with the smearing parameter $r' = 0.188$ mkm in (29).

To reconstruct the function $z(x_1, x_2)$ for backscattered data given in Figure 1-a) we apply the adaptive algorithm of Section 8. First, we compute the function z_0 on a coarse mesh T_0 for $k = 0$ with the regularization parameter $\alpha =$ 3e10−07 in (33). The coarse mesh T_0 is presented in Figure 1-g).

Now we describe our stopping criterion for the mesh refinements. According to the second mesh refinement recommendation we refine the mesh in all subdomains where the function $B_h(z_k)$ attains its maximal values or where

$$|B_h(z_k)| \geq \beta_k \max_\Omega |B_h(z_k)| \quad (36)$$

with $\beta_k = 0.5$. Next, we perform all the steps of the first adaptive algorithm of Section 8 until the desired tolerance $\|z_k - z_{k-1}\| < \epsilon$ with $\epsilon =$ 10e − 05 is achieved, or the computed L_2-norms of the differences $\|z_k - z_{k-1}\|$ start to grow abruptly.

Figures 1-b)-f) show results of the reconstruction of the function $z(x_1, x_2)$ on the adaptively refined meshes presented in Figures 1-h)-l). We observe that on the fifth refined mesh corresponding to Figure 1-l) we obtain the best restoration results. Since the computed L_2-norms $\|z_k - z_{k-1}\|$ with $k = 5$ start to grow abruptly after the fifth refinement of the initial mesh we conclude that the function z_5 of Figure 1-f) is our final reconstruction result.

Test 1-b). This test is similar to the previous one only the goal was to reconstruct the function $z(x_1, x_2)$ in (32) using backscattered data $u(\xi, \eta)$ presented in Figure 2-a). The computational domain Ω in this test is the same as in Test 1-a). The backscattered signal of Figure 2-a) is the simulated function $u(\xi, \eta)$ with the same smearing parameter $r' = 0.188$ mkm in (29) as in Test 1-a).

To reconstruct the function $z(x_1, x_2)$ we apply the second adaptive algorithm of Section 8 with both the mesh refinement recommendations of Section 7. Figures 2-b)-c) show results of the reconstruction of the function $z(x_1, x_2)$ on the adaptively refined meshes presented in Figures 2-e)-f). Stopping criterion for mesh refinements are the same as in Test 1-a).

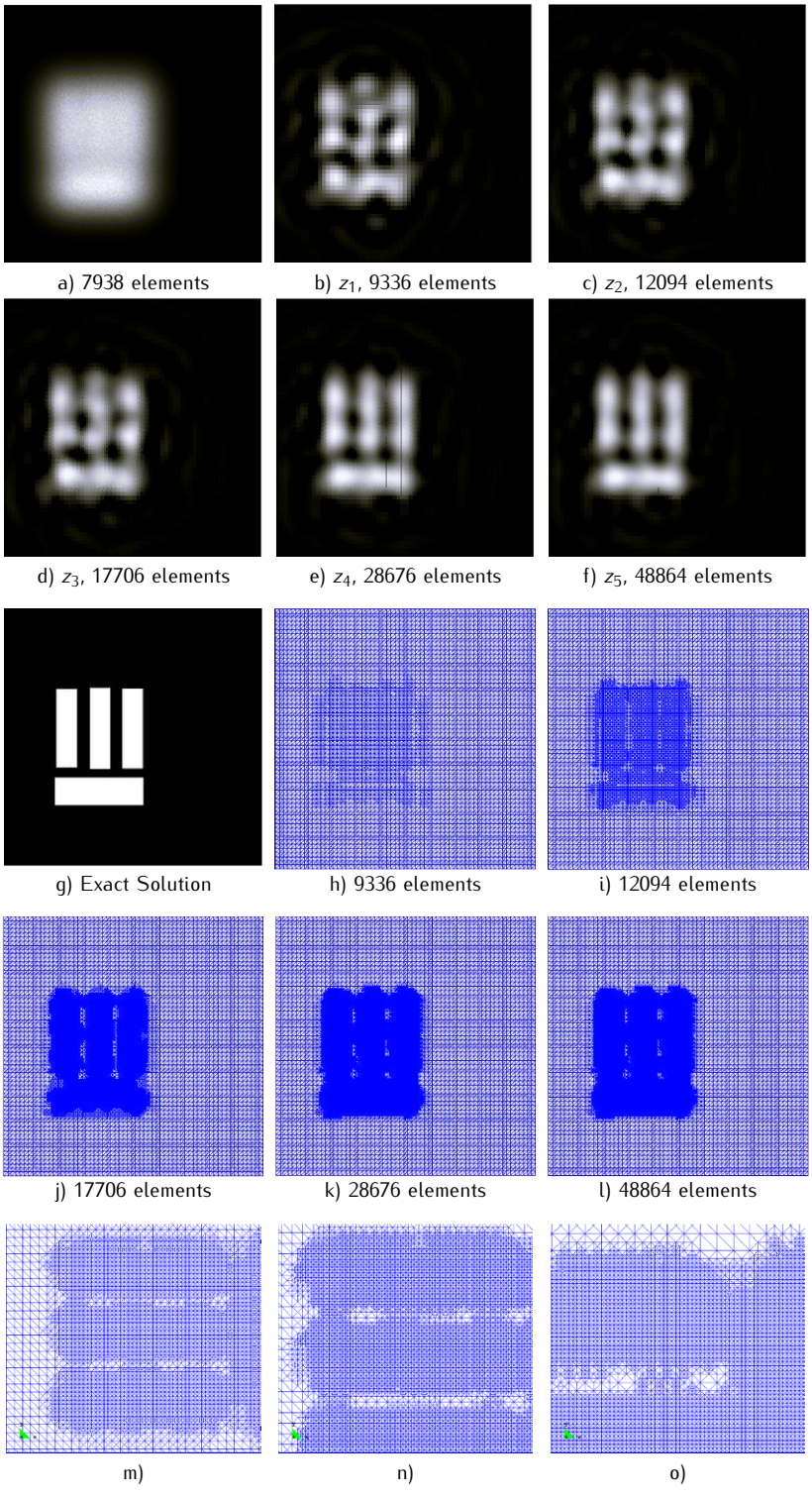

Figure 1. Test 1-a). Reconstruction of the function $z(x_1, x_2)$ using simulated backscattered data. In a) we present simulated backscattered data $u(\xi, \eta)$. In b)–f) we show results of the reconstruction of the function $z(x_1, x_2)$ on different adaptively refined meshes using the algorithm of Section 8 and in g) we present the known exact function z^*. Adaptively refined meshes corresponding to images c)–f) are presented in h)–l). Enlarged parts of the refined meshes in j), k), l) are presented in m), n), o), respectively.

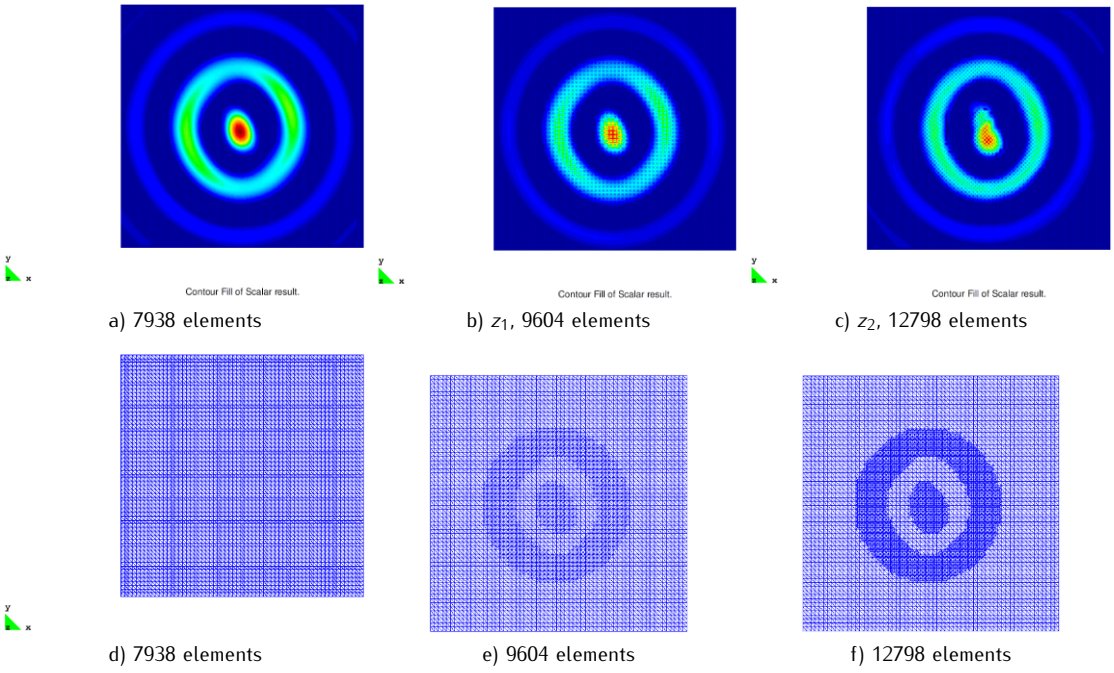

a) 7938 elements b) z_1, 9604 elements c) z_2, 12798 elements

d) 7938 elements e) 9604 elements f) 12798 elements

Figure 2. Test 1-b). Reconstruction of the function $z(x_1, x_2)$ using simulated backscattered data. In a) we present simulated backscattered data $u(\xi, \eta)$. In b)–f) we show results of the reconstruction of the function $z(x_1, x_2)$ on the different adaptively refined meshes using the second algorithm of Section 8. Adaptively refined meshes corresponding to images b)–c) are presented in e)–f).

We observe that on the second refined mesh corresponding to Figure 2-f) we obtain the best restoration results. Since the computed L_2-norms $\|z_k - z_{k-1}\|$ start to grow abruptly after the second refinement of the initial mesh we conclude that the function z_2 of Figure 2-c) is our final reconstruction result.

Test 2. The goal of this test is to present the efficiency and robustness of applying the adaptive mesh refinement for calculating the deconvolution function z_α given by (34). The computational domain Ω in this test has the area $S_\Omega = 6.963\,\text{mkm}$. The backscattered signal is the simulated function $u(\xi, \eta)$ in (32) which is presented in Figure 3-a). This function is computed for the function $\rho(x_1 - \xi, x_2 - \eta)$ with the smearing parameter $r' = 0.0612\,\text{mkm}$ in (29). In Figure 3-b) we present the computed deconvolution function z_α on the adaptively refined mesh using the first adaptive algorithm of Section 8, with the small regularization parameter $\alpha = 2e10-7$ in the Tikhonov functional (33). Figure 3-c) shows the computed deconvolution function z_α on the uniform mesh with the regularization parameter $\alpha = 0.01$ in the Tikhonov functional (33). Figure 3-d) shows that the image blows up for the uniform mesh taking the small regularization parameter $\alpha = 2e10-7$ in the Tikhonov functional (33).

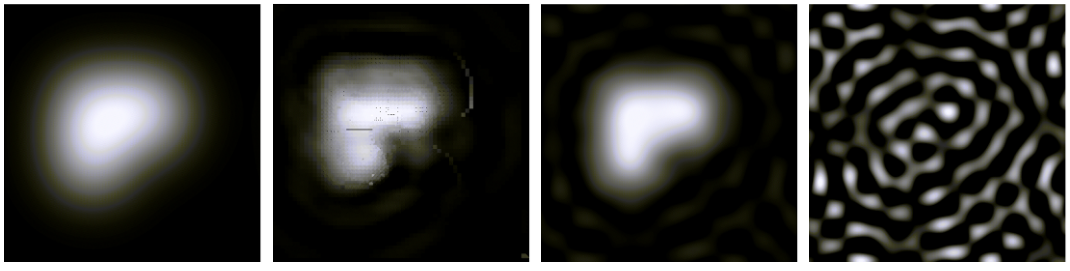

a) b) c) d)

Figure 3. Test 2. Efficiency of the application of the adaptive mesh refinement for calculation of the deconvolution function z_α, given by (34). a) Simulated backscattered data $u(\xi, \eta)$. b) Computed deconvolution function z_α on the adaptively refined mesh with the regularization parameter $\alpha = 2e10-7$. c), d) Computed deconvolution function z_α on the uniform mesh with the regularization parameters $\alpha = 0.01$ and $\alpha = 2e10-7$, respectively.

Comparing the results in Figure 3 we can conclude that the computed deconvolution function z_α on the adaptively refined mesh of Figure 3-b) is better than the corresponding function on the uniform mesh of Figure 3-c). We observe that this function blows up for the uniform mesh when the regularization parameter is taken to be the same as in the adaptive algorithm, when comparing Figure 3-b) with Figure 3-d). This test highlights the robustness of using the adaptive algorithm for image restoration problems.

9.3. Tests with experimental data. Test 3

In this test our goal was to solve (**IP**) and restore the function $z(x_1, x_2)$ in (32) using experimentally measured backscattered data $u(\xi, \eta)$ and the known function $\rho(x_1 - \xi, x_2 - \eta)$ in (32). The computational domain Ω in this test has the area $S_\Omega = 16.963$ mkm and represents part of the planar microscheme. In Figure 4-a) we show the backscattered signal $u(\xi, \eta)$ obtained from the experimentally measured data by microtomograph [18, 23]. This function was measured at depth $d = 0.9\,\mu$m of the microscheme with the smearing parameter $r' = 0.149$ mkm in (29).

To reconstruct the function $z(x_1, x_2)$ from backscattered data given in Figure 4-a) we apply the first adaptive algorithm of Section 8. First, we compute z_0 using the finite element discretization of (34) with the regularization parameter $\alpha = 2e10 - 07$ in (33) on the coarse mesh presented in Figure 4-g). Then we refine the mesh in all subdomains where the gradient of (35) attains its maximal values by choosing $\beta_k = 0.5$ in (36). Next, we perform all steps of the adaptive algorithm until the desired tolerance $\|z_k - z_{k-1}\| < \epsilon$ with $\epsilon = 10e - 05$ is achieved or the computed L_2- norms of the differences $\|z_k - z_{k-1}\|$ start to grow abruptly.

Figures 4-b)-f) show the results of the reconstruction of the function $z(x_1, x_2)$ on the adaptively refined meshes which are presented in Figures 4-h)-l). We observe that on the fifth refined mesh corresponding to Figure 4-l) we obtain the best reconstruction results. Since the computed L_2-norms $\|z_k - z_{k-1}\|$ start to grow abruptly after the fifth refinement of the initial mesh we conclude that the function z_5 of Figure 4-f) is our final reconstruction result.

9.4. Comparison with other methods. Test 4

In this subsection we present a performance comparison between three different reconstruction methods: the adaptive finite element method of this paper, the uniform grid deconvolution method on the Sobolev space H^1 of [23] and the Bounded Total Variation method VH of [18].

In all our tests we solve (**IP**) and reconstruct the function $z(x_1, x_2)$ in (32) using the backscattered function $u(\xi, \eta)$ given in Figure 1-a) and known function $\rho(x_1 - \xi, x_2 - \eta)$ in (32). The computational domain Ω in this test is the same as in Test 1. We perform two different set of tests: in Test 4-a) we use simulated computational data with different noise levels (we apply additive white Gaussian noise where the maximal amplitude I_a is varied on the interval $I_a = [0\,\%, 100\,\%]$), and in Test 4-b) we use different values of the smearing parameter $r'(d)$ such that it belongs to the interval $r'(d) = [0, 0.3 \cdot l]$, where l is the linear size of the frame under investigation.

Our analysis is based on calculating of relative error e_r

$$e_r = \frac{\|z^* - z_\alpha\|^2_{L_2(\Omega)}}{\|z^*\|^2_{L_2(\Omega)}}. \tag{37}$$

Here, z^* defines the exact solution and z_α is the computed solution to (**IP**). Note that to compute the relative error in (37) we used the known exact solution z^* presented in Figure 1-g).

Test 4-a). Figure 5 shows performance comparison of three methods. Using Figure 5 (left) we observe that the Bounded Total Variation method gives the best performance results in Test 4-a) with this method giving the smallest relative error e_r for increasing noise levels. We also observe that an adaptive finite element method performs better than the uniform grid deconvolution method with increasing noise levels in the computational data. In this test an adaptive finite element method was applied with the piecewise-constant function in the finite element approximation of the function $z(x_1, x_2)$. We are planning to check performance of an adaptive finite element method with a higher polynomial approximation of this function in future research.

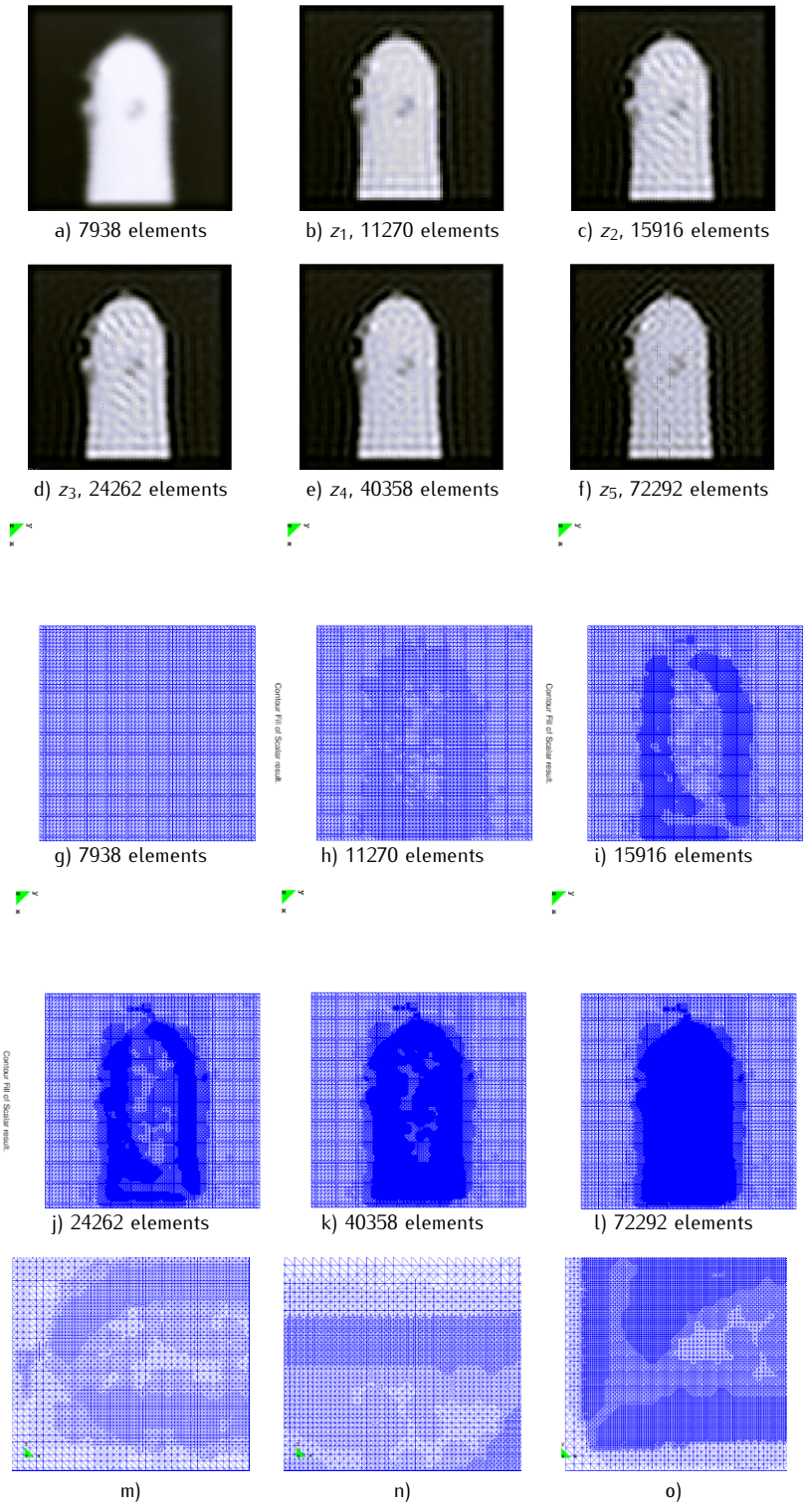

Figure 4. Test 3. Reconstruction of the function $z(x_1, x_2)$ from the experimental backscattering data obtained by the microtomograph [18, 23]. In a) we present the real measured signal $u(\xi, \eta)$ on the part of the planar microscheme Ω obtained by the microtomograph at the depth 0.9 μm. In b)–f) we show results of the reconstruction of the function $z(x_1, x_2)$ on different adaptively refined meshes using the algorithm of Section 8. Adaptively refined meshes corresponding to images b)–f) are presented in h)–l). Enlarged parts of refined meshes in j), k), l) are presented in m), n), o) respectively.

Test 4-b). Figure 5 (right) shows the performance results of the three reconstruction methods when using different values of the smearing parameter $r'(d)$ in computations. We observe that the smallest relative error we obtain using the adaptive finite element method is when the function $r'(d)$ has a high intensity ($r'(d) > 0.2$). We can conclude that an adaptive FEM performs better than other two methods in the case of the reconstruction of high-intensive smeared images.

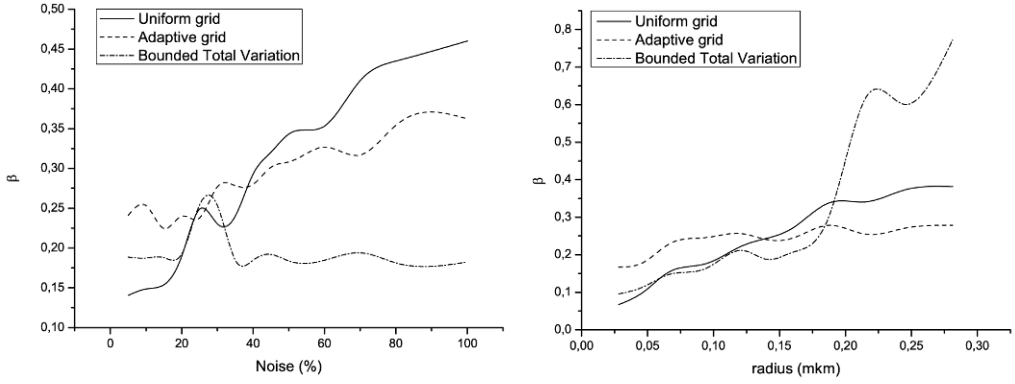

Test 4-a) Test 4-b)

Figure 5. Test 4. Performance comparison of an adaptive finite element method, uniform grid deconvolution method and Bounded Total Variation method.

10. Conclusions

In this work we considered solving a Fredholm integral equation of the first kind (3) as an ill-posed problem (**P**). To find a regularized solution z_α to (**P**) we minimized the Tikhonov functional (6) on adaptivelly refined meshes. To do this we used CG(1) and DG(1) finite element methods to solve the minimization problem (10). We derived a posteriori error estimates for the error in the regularized solution z_α of the Tikhonov functional (6) in Theorem 5.1 and for the error in Tikhonov functional (6) in Theorem 6.1. Both theorems are valid for the case of a more general functional (9). Using these theorems we formulated local mesh refinement recommendations which improve the accuracy of the reconstruction of the regularized solution z_α in the Tikhonov functionals (6) and (9). Our two-dimensional numerical experiments of Section 9 justify the efficiency of our a posteriori estimates applied both to the computationally simulated and experimental backscattered data measured in microtomography.

Acknowledgements

This research was supported by the Swedish Research Council, the Swedish Foundation for Strategic Research (SSF) through the Gothenburg Mathematical Modelling Center (GMMC) and by the Swedish Institute, Visby Program. The first author acknowledges also the Russian Foundation For Basic Research, the grant RFFI 11-01-00040.

References

[1] Asadzadeh M., Eriksson K., On adaptive finite element methods for Fredholm integral equations of the second kind, SIAM J. Numer. Anal., 1994, 31(3), 831–855

[2] Atkinson K.E., The numerical solution of integral equations of the second kind, Cambridge Monogr. Appl. Comput. Math., 4, Cambridge University Press, Cambridge, 1997
[3] Bakushinsky A.B., A posteriori error estimates for approximate solutions of irregular operator equations, Dokl. Math., 2011, 83(2), 192–193
[4] Bakushinsky A.B., Kokurin M.Yu., Smirnova A., Iterative Methods for Ill-Posed Problems, Inverse Ill-Posed Probl. Ser., 54, Walter de Gruyter, Berlin, 2011
[5] Basistov Yu.A., Goncharsky A.V., Lekht E.E., Cherepashchuk A.M., Yagola A.G., Application of the regularization method for increasing of the radiotelescope resolution power, Astronomicheskii Zhurnal, 1979, 56(2), 443–449 (in Russian)
[6] Beilina L., Klibanov M.V., A posteriori error estimates for the adaptivity technique for the Tikhonov functional and global convergence for a coefficient inverse problem, Inverse Problems, 2010, 26(4), #045012
[7] Beilina L., Klibanov M.V., Reconstruction of dielectrics from experimental data via a hybrid globally convergent/adaptive inverse algorithm, Inverse Problems, 2010, 26(12), #125009
[8] Beilina L., Klibanov M.V., Kokurin M.Yu., Adaptivity with relaxation for ill-posed problems and global convergence for a coefficient inverse problem, J. Math. Sci. (N.Y.), 2010, 167(3), 279–325
[9] Beilina L., Klibanov M.V., Kuzhuget A., New a posteriori error estimates for adaptivity technique and global convergence for the hyperbolic coefficient inverse problem, J. Math. Sci. (N.Y.), 2011, 172(4), 449–476
[10] Bolotina A.V., Luk'yanov F.A., Rau E.I., Sennov R.A., Yagola A.G., Energy spectra of electrons backscattered from bulk solid targets, Moscow University Physics Bulletin, 2009, 64(5), 503–506
[11] Eriksson K., Estep D., Johnson C., Applied Mathematics: Body and Soul, 3, Springer, Berlin, 2004
[12] Goncharsky A.V., Cherepashchuk A.M., Yagola A.G., Ill-Posed Problems of Astrophysics, Moscow, Nauka, 1985 (in Russian)
[13] Groetsch C.W., Inverse Problems in the Mathematical Sciences, Vieweg Math. Sci. Engrs., Friedr. Vieweg & Sohn, Braunschweig, 1993
[14] Johnson C., Numerical Solution of Partial Differential Equations by the Finite Element Method, Dover, Mineola, 2009
[15] Johnson C., Szepessy A., Adaptive finite element methods for conservation laws based on a posteriori error estimates, Comm. Pure Appl. Math., 1995, 48(3), 199–234
[16] Klibanov M.V., Bakushinsky A.B., Beilina L., Why a minimizer of the Tikhonov functional is closer to the exact solution than the first guess, J. Inverse Ill-Posed Probl., 2011, 19(1), 83–105
[17] Koshev N.A., Luk'yanov F.A., Rau E.I., Sennov R.A., Yagola A.G., Increasing spatial resolution in the backscattered electron mode of scanning electron microscopy, Bulletin of the Russian Academy of Sciences: Physics, 2011, 75(9), 1181–1184
[18] Koshev N.A., Orlikovsky N.A., Rau E.I., Yagola A.G., Solution of the inverse problem of restoring the signals from an electronic microscope in the backscattered electron mode on the class of bounded variation functions, Numerical Methods and Programming, 2011, 12, 362–367 (in Russian)
[19] Kress R., Linear Integral Equations, Appl. Math. Sci., 82, Springer, Berlin, 1989
[20] Tikhonov A.N., Goncharsky A.V., Stepanov V.V., Kochikov I.V., Ill-posed problems of image processing, Soviet Phys. Dokl., 1987, 32(6), 456–458
[21] Tikhonov A.N., Goncharsky A.V., Stepanov V.V., Yagola A.G., Numerical Methods for the Solution of Ill-Posed Problems, Math. Appl., 328, Kluwer, Dordrecht, 1995
[22] Tikhonov A.N., Leonov A.S., Yagola A.G., Nonlinear Ill-Posed Problems, Appl. Math. Math. Comput., 14, Chapman & Hall, London, 1998
[23] Yagola A.G., Koshev N.A., Restoration of smeared and defocused color images, Numerical Methods and Programming, 2008, 9, 207–212 (in Russian)